Nuclear Instruments and Methods in Physics Research 224 (1984) 532–546
North-Holland, Amsterdam

DESIGN AND CALIBRATION OF AN ABSOLUTE FLUX DETECTOR FOR 1–15 MeV NEUTRONS

Mauro S. DIAS, * Ronald G. JOHNSON and Oren A. WASSON

National Bureau of Standards, Washington, DC 20234, USA

Received 18 October 1983 and in revised form 23 January 1984

An absolute neutron flux monitor having fast timing and a calculable response has been developed for use in a collimated beam of 1–15 MeV neutrons. The detector consists of dual thin plastic scintillators in which the proton recoil spectrum distortion caused by the escape of protons from the first scintillator is eliminated experimentally. The absolute detector efficiency was measured at 2.45 and 14.0 MeV neutron energies using the associated-particle technique at the NBS Positive-Ion Van de Graaff facility. The efficiency and pulse height distributions were calculated using a Monte Carlo based program in order to extend the efficiency throughout the 1–15 MeV interval. The uncertainty in the efficiency is 1–2% (1 standard deviation).

1. Introduction

There is a continuing need for absolute neutron flux detectors having fast timing and a calculable simple response with neutron energy. Organic scintillators have been extensively used as neutron flux monitors employing the proton recoil technique. In order to keep multiple scattering corrections small, thin scintillators are required. However, for thin scintillators and neutrons of several MeV the escape of protons from the scintillator produces a large distortion in the proton recoil spectrum. A detector which reduces this distortion has been designed and calibrated at the National Bureau of Standards for use in neutron cross section experiments with the NBS 150 MeV Electron Linac and 3 MV Positive-Ion Van de Graaff accelerator.

In the present work a dual thin scintillator detector for use in a collimated neutron beam is described where the escape of protons is eliminated experimentally and the multiple scattering is low. The detector consists of two thin plastic scintillators optically separated from each other and independently coupled to phototubes. The protons which escape from the first scintillator are detected by the second scintillator which is placed behind the first. Because of the low multiple scattering and the spectrum discrimination, there is relatively little dependence of the detector efficiency on the carbon cross section and angular distributions. Therefore the detector efficiency is essentially dependent on the hydrogen cross section, which is known with accuracies $\lesssim 1\%$, on light tables, and on hydrogen areal density. These are parameters that can be verified experimentally.

The absolute detector efficiency was measured at 2.45 and 14.0 MeV using the associated-particle technique with the NBS Positive-Ion Van de Graaff as the neutron source. Details of these experiments are described in section 4. Theoretical calculations of the detector's absolute efficiency and pulse height distributions have been performed using a Monte Carlo code. Details of the calculations are found in section 5. Using these calculations the detector's absolute efficiency is determined from 1 to 15 MeV. The principles of the detector's operation and details on the detector's design are contained in sections 2 and 3, respectively.

2. Principles of detector operation

The present detector was designed to be used as an absolute neutron flux monitor in accurate neutron cross section measurements using the NBS 3 MV Positive-Ion Van de Graaff and the 150 MeV Electron Linac as the sources of neutrons. The desired characteristics for such a detector were: (a) a detection efficiency which has a simple dependence on the neutron energy; (b) small efficiency corrections [1] in order to obtain the absolute efficiency with 1–2% uncertainty; (c) fast time response; (d) an energy range for neutron fluxes of 1–15 MeV; (e) a geometry which did not require the use of precision collimators.

The first three requirements have been achieved by using the detection of proton recoils in an organic scintillator whose thickness was chosen to be small compared to the neutron mean free path. In this case, the proton recoil energy spectrum approaches the ideal

* Permanent address: Instituto de Pesquisas Energéticas e Nucleares, São Paulo, Brazil.

rectangular shape if edge effects are neglected. However, at neutron energies of several MeV the escape of protons through the forward edge of the scintillator produces a large distortion in the proton recoil spectrum. The distorted spectrum in the first scintillator was calculated on the basis of the equations given in ref. [1]. In this estimate, it was assumed that

$$R(E) = KE^{3/2}, \tag{1}$$

where $R(E)$ is the proton range at energy E and K is a constant. The distorted spectrum is given by:

$$N'_p(E) = N_p(E)\left\{1 + \frac{R_0}{2L}\left[1 - 3\left(\frac{E}{E_0}\right)^2\right]\right\}, \tag{2}$$

where

$N_p(E)$ is the undistorted spectrum (curve A of fig. 1),
R_0 is the proton range at $E = E_0$,
L is the thickness of the scintillator, and
E_0 is the incident energy.

This distorted spectrum is shown for $L = 0.254$ cm and for 14 MeV neutrons in curve A' of fig. 1. In this case the fraction of escaped protons amounts to 30% of the spectrum.

In the present detector, the distortion due to the escape of protons is eliminated experimentally by the use of a dual thin scintillator configuration as shown in fig. 2. A proton which escapes deposits part of its energy in scintillator 1 and part in scintillator 2. Therefore the sum of the light outputs produced in each scintillator corresponds to the total energy of the recoil proton. The sum spectrum is given by:

$$N'_{p_s}(E) = N_p(E)\frac{R_0}{L}\left(\frac{E}{E_0}\right)^2. \tag{3}$$

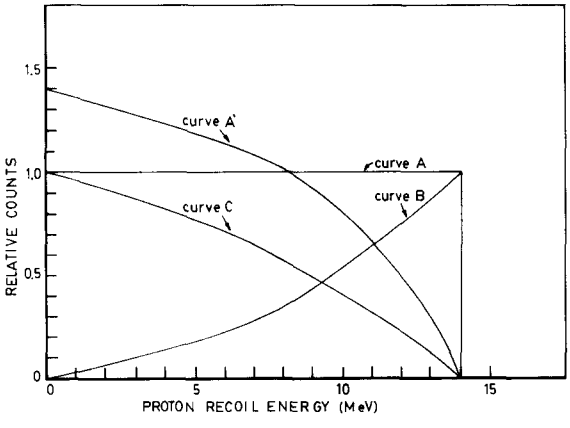

Fig. 1. Effect of the escape of protons on the proton recoil energy distribution at 14 MeV. Curve A': proton recoils in a single thin scintillator. Curve B: proton recoils that escape from scintillator 1, therefore, losing part of their energy in scintillator 2. Curve C: proton recoils completely absorbed in scintillator 1. Curve A = B + C: ideal rectangular distribution.

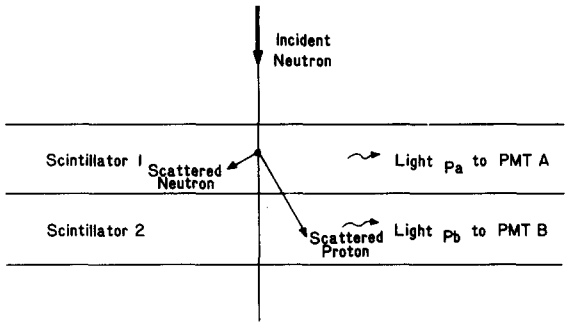

Fig. 2. Light produced by a recoil proton in the dual thin scintillator detector.

This spectrum is shown as curve B in fig. 1. These events are identified experimentally through a coincidence requirement. Protons that lose all their energy in scintillator 1 are also included in the spectrum. The spectrum for these protons is given by:

$$N'_{p_T}(E) = N_p(E)\left[1 - \frac{R_0}{L}\left(\frac{E}{E_0}\right)^2\right]. \tag{4}$$

This spectrum is represented by curve C in fig. 1.

The summation of spectrum B and spectrum C approaches the ideal thin scintillator response. This corresponds to:

$$N_p(E) = N'_{p_s}(E) + N'_{p_T}(E). \tag{5}$$

This summation produces the spectrum shown as curve A in fig. 1. Signals produced by neutrons detected only in the second scintillator are rejected because of the coincidence requirement.

3. Detector design

The main aspects considered in the detector design are: irradiation geometry, scintillator type, dimensions, and light collection geometry.

3.1. Irradiation geometry

Because thin scintillators are used, the present detector has a high transmission over the neutron energy range considered. Therefore it was decided to have the phototubes view the scintillators from the side as shown in fig. 3, so that the neutron beam is only attenuated by the scintillators. In this way the detector can be used in transmission geometry when desired.

A disc-shaped plastic scintillator was glued into a circular hole in a rectangular plexiglas light guide. The thickness of the light guide was chosen equal to the scintillator thickness so that most of the light that

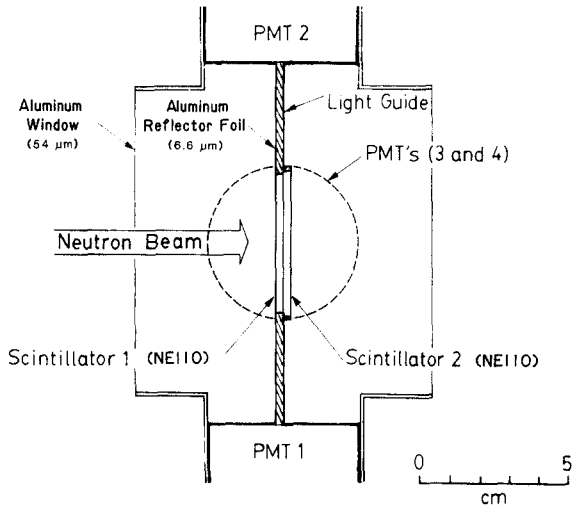

Fig. 3. Geometry of the dual thin scintillator detector.

reaches the photocathode is by total internal reflection. The main advantages of this geometry are: the possibility of using the scintillator totally immersed in the neutron beam when desired; a lower background when compared to a rectangular scintillator without light guide; and a simple geometry for efficiency and spectrum calculations. Further advantages of this geometry are that the edge effect at the side of the scintillator can be reduced by using a diameter sufficiently large and there is better light collection uniformity at different points in the scintillator (see section 3.3).

3.2. Scintillator type and dimensions

NE110 plastic scintillator was chosen because of its well known properties of good light transmission and high light output [2]. Also it can be easily machined to the desired shape. NE110 is a polyvinyl toluene based plastic, having concentrations of 0.05233 hydrogen atoms/b · cm and 0.04736 carbon atoms/b · cm. The other elements present are: 1.8×10^{-6} nitrogen atoms/b · cm and 1.8×10^{-6} oxygen atoms/b · cm. The use of a scintillator that also provides pulse shape discrimination against gamma rays (e.g., stilbene) was not attempted because in the present application the signals due to gamma rays were eliminated by using coincidence or time-of-flight techniques.

For a disc-shaped scintillator, the two dimensions to consider are thickness and diameter. Since scintillator 2 detects the proton recoils which escape from scintillator 1, its thickness must be greater than the maximum proton range. Using the relationships from Cecil et al. [3] (for the range–energy data [4]) the maximum proton range corresponding to 15 MeV protons is equal to 0.246 cm. A convenient thickness was found to be 0.2565 cm. A larger value is not desirable because it would increase the multiple scattering correction.

The thickness of the first scintillator is a compromise between neutron detection efficiency and multiple scattering corrections. This thickness which was chosen to be the same as the second scintillator (0.2565 cm) turned out to have a reasonable efficiency (~ 3% at 2.45 MeV and ~ 0.7% at 14.0 MeV, which is much larger than the usual proton recoil telescopes [5]). An additional advantage in having both scintillators with the same thickness is to have the same proton recoil spectrum shapes, making it easier to match the relative output gains of each scintillator. The thickness has been accurately measured (± 0.0005 cm) at different points in the scintillator in order to determine the efficiency for any size neutron beam.

For the dual scintillator configuration chosen for the detector, and for the above dimensions, the multiple scattering correction above a selected spectrum bias were 11% at 2.45 MeV and 4% at 14.0 MeV. These values were not expected to introduce unacceptable uncertainties in the calculated detector efficiency.

The scintillator diameter was defined using two criteria: (1) detector calibration geometry at the NBS Van de Graaff, and (2) escape of protons through the sides of the scintillator. As discussed in sections 4.2 and 4.3, the detector diameter must be greater than the size of the associated neutron cone for the two calibration energies, namely 2.45 and 14.0 MeV. Secondly, the escape of protons through the sides of the scintillator should be a small correction to be applied when the whole scintillator is immersed in a neutron beam. The correction for this effect was estimated using the following relationship:

$$S = \frac{1}{4}\frac{R(E)}{r}\left[1 - \frac{E}{E_0}\right]^{1/2}, \tag{6}$$

where $R(E)$ is the scattered proton range at energy E and r is the scintillator radius. A convenient diameter was chosen to be 4.70 cm for scintillator 1 corresponding to a 0.8% correction for escape of protons through the side of the scintillator at 15 MeV incident neutron energy. This diameter has an additional advantage of being about the same size as the photocathode of the RCA 8850 photomultiplier tube (PMT) which was readily available. A slightly larger diameter of 4.90 cm was chosen for scintillator 2 in order to detect the escape protons from the edge of scintillator 1.

3.3. Light collection geometry

A series of measurements of light collection efficiency and uniformity were performed using a ^{137}Cs collimated gamma source. For this experiment a rectangular NE110 scintillator (0.254 cm × 5.3 cm × 6.0 cm) coupled to two RCA 8850 photomultiplier tubes through

the shorter sides was used. (These measurements were performed early in the development of the detector to provide information for the final design.) Aluminum foils 6.6 μm thick were wrapped around the scintillator in order to produce better light collection uniformity for this geometry [6]. Aluminized mylar, although it is a slightly better reflector [7], was not used because it would produce undesired proton recoils in the scintillator when used in a neutron beam. In the interface between the two scintillators 0.66 μm thick aluminum foils were used as reflectors. With this thickness the energy loss by recoil protons in the reflectors will be negligible (see section 5.7). The phototubes and scintillators were held together inside a box that has a 54 μm thick aluminum window on each side in order to make the system light tight.

A 1.0 mm thick plexiglas plus a 0.30 mm thick Pb filter was placed in front of the collimated source in order to prevent X-rays or conversion electrons from reaching the detector. The gamma ray beam profile was measured by displacing the detector so that only a fraction of the beam was incident on the scintillator. The analysis showed an average beam diameter of 1.1 cm with no appreciable penumbra. In this series of measurements, the detector was scanned to determine the channel position of the 50% height of the Compton spectrum edge for five different positions along the phototubes axis. Spectra from each individual PMT were measured as well as the sum spectra. The results using the optical coupling compound Dow Corning 02.3067 on both scintillator edges are shown in fig. 4 (condition I). The results obtained using air coupling, i.e., laying the scintillator edge against the photocathode glass, are shown in fig. 4 (condition II). From these measurements it was concluded that the conditions of best light collection uniformity for each individual PMT is obtained when the scintillator is attached to the photocathode glass using air coupling. This is due to the contribution of reflected light from the opposite edge of the scintillator. The sum of pulses from both PMTs results in the highest light collection efficiency. Because the pair of PMTs are placed on opposite sides, the sum of signals partially compensates for the variation in the light collection from the individual PMTs. This results in the best light collection uniformity for different points in the scintillator, as shown by curves C in fig. 4.

Although a satisfactory uniformity in the light collection was obtained in the PMTs axial direction, large variations were observed in the direction perpendicular to the PMTs axis. The variations were as high as 9% at different points on the scintillator. These variations were caused by differences in the photocathode sensitivity, as well as by the geometric solid angle between each point in the scintillator and the photocathode. For this reason it was decided to use a longer light guide in order to minimize these effects without much loss in light collection efficiency. A rectangular plexiglas light guide measuring 5.3 cm × 12.0 cm, with a circular hole in the

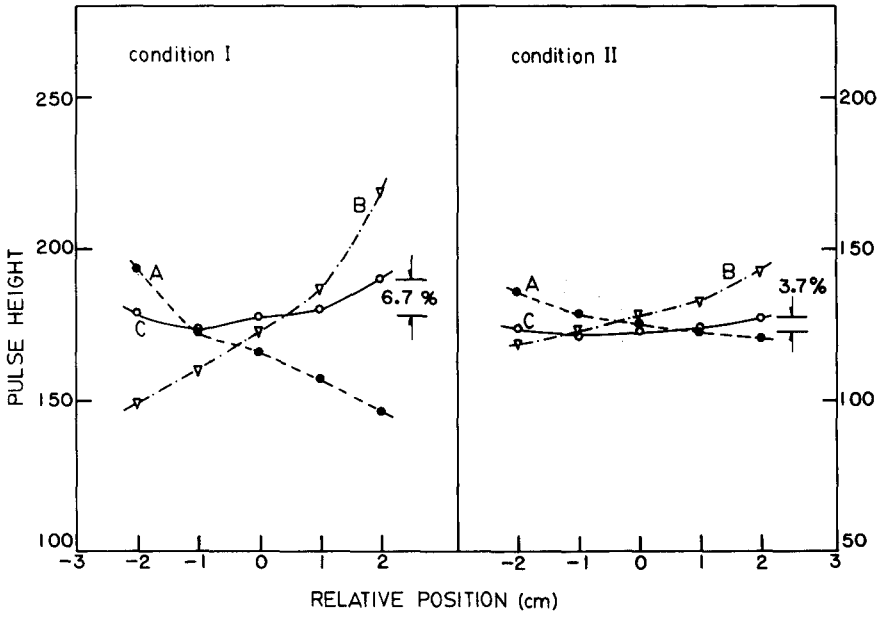

Fig. 4. Variation in light collection as a function of radial position in the scintillator. Curves A and B: Single photomultiplier tube (PMT) response. Curve C: sum of both PMT responses. Condition I: scintillator edges with optical compound Dow Corning 02.3067. Condition II: scintillator edges with air coupling.

center in which the scintillator was attached with clear epoxy was chosen. The resulting geometry is shown in fig. 3.

With this geometry, the uniformity of light collection was measured to be better than 2.5% per cm for scintillator 1 and better than 1.3% per cm for scintillator 2 for points around the center of the scintillators. From these results it is expected that the variation in light collection at different points would produce only small distortions in the proton recoil spectrum for the detector.

Radiation incident on the light guide produced a negligible ($< 0.5\%$) contribution to the detector response. This was determined from measurements of the integrated counting rate produced by the gamma ray beam incident on the light guide.

4. Experimental detector efficiency calibration

Checks of the absolute efficiency of the detector were performed by means of the associated-particle technique at the NBS 3 MV Positive-Ion Van de Graaff. For this purpose, a monoenergetic 500 keV deuterium molecular ion beam (D_2^+) was utilized. The deuterium molecular ion dissociates upon impact with the target allowing a 250 keV atom to interact with the target nuclei. The reactions T(d, n)^{4}He and D(d, n)^{3}He were used to generate neutrons with 14.0 and 2.45 MeV, respectively. Details of the measurements are given in the following sections.

4.1. Electronics for the neutron detector calibration

A simplified block diagram of the electronics developed for the neutron detector is shown in fig. 5. Each scintillator was coupled to a pair of RCA 8850 PMT, chosen for their high gain, low noise, and convenient size. Three layers of high μ metal 0.18 mm thick each were wrapped around each PMT to provide a good magnetic and electrostatic shielding. The four PMTs received the high voltage from a single power supply, minimizing any relative gain variation between each PMT. The gain stability of the system was measured for individual scintillators in a 14 MeV neutron beam and showed a stability better than ~ 0.7% over a period of three days. For each photomultiplier both time and linear signals were derived. The linear signals from the pair of each scintillator were added in a passive mixer consisting of 20 kΩ resistors and then fed into a charge sensitive preamplifier (PA) and shaping amplifier (AMP) system. After adjusting for the proper delays the signals from each amplifier were joined in a sum amplifier. A linear gate placed in the second scintillator leg was triggered by the timing signal from the first scintillator; therefore all single events from the second scintillator were rejected. The pulses from the sum amplifier are single events from the first scintillator plus sum pulses produced by coincident events between the two scintillators.

A 0.25 μs time constant was selected for the neutron amplifier to provide a unipolar output pulse with a 0.6 μs full width at half-maximum (fwhm). A fast amplifier and constant fraction discrimination (CFD) were used to provide good timing for the neutron detector. The FAN-IN and fast amplifier combination resulted in high amplification of the PMT signal, which was necessary in order to minimize the effect of loss of coincidence events between the two scintillators due to pulses occurring below the CFD lower level. This effect was verified by measuring the neutron detector efficiency for different settings of the CFD lower level.

The alpha particle signals from the solid state detec-

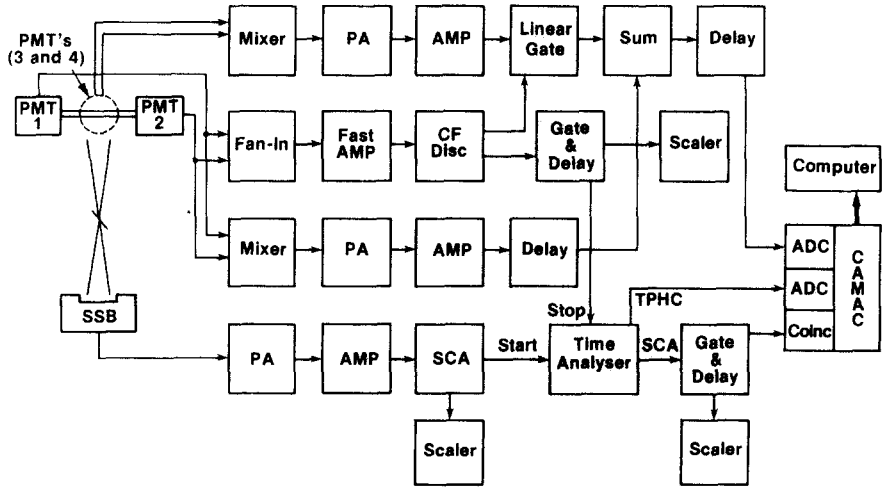

Fig. 5. Electronics for the neutron detector calibration.

tor were also fed to a charge sensitive preamplifier and shaping amplifier system. A bipolar output shape was used in order to provide a better time resolution from the single channel analyzer.

The time distribution between the alpha particle and neutron events was measured with a time analyzer. The measured coincidence-resolving times were 5–10 ns which are adequate for these measurements. Since the alpha rate ($\sim 1500\ s^{-1}$) was lower than the neutron detector rate ($\sim 4000\ s^{-1}$), the alpha signal was used as the start signal. The analog signal from the sum amplifier of the neutron flux detector was fed into an analog to digital converter (ADC). Another ADC was used to receive the signals from the time analyzer. The data from both ADCs were then transferred through a CAMAC interface into a 32×128 word array in the computer for storage. A two-parameter unit was used having 32 time channels with a width of 32 ns per channel.

4.2. Calibration at 14.0 MeV

The NBS 14 MeV absolute neutron beam facility is described in refs. [8] and [9]. A view of the experimental geometry is shown in fig. 6. The molecular ion beam D_2^+ was collimated to a 3 mm diameter providing ~ 0.1 μA current onto a 2.8 mg/cm^2 thick TiT target. The 3.6 MeV ^{4}He associated particle produced in the T(d, n)^{4}He reaction was detected by a 150 μm thick surface barrier detector located at an 85° angle with respect to the beam axis and 14.6 cm away from the target. The ^{4}He detector was collimated to a 3.8° cone angle. In these conditions the ^{4}He counting rate was $\sim 1500\ s^{-1}$. A 2.3 mg/cm^2 thick nickel foil was mounted over the collimator in order to reduce the background from elastic scattered deuterons and beta particles from the decay of tritium in the target. The background in the alpha particle detector was measured in a separate run by insertion of a 0.03 mm thick aluminum foil over the surface of the detector. The background was due to deuteron interactions with the titanium and neutron induced reactions in the silicon surface barrier detector. The background due to charged particles from the ^{3}He(d, p)^{4}He and ^{2}H(d, p)^{3}H reactions did not contribute significantly to the detector rate.

The neutrons were detected at 90° and 99% of the associated neutron flux was contained in a cone with a 6.0° half-angle. The cone subtended by the NE110 scintillators in the neutron flux detector had a 10.9° half-angle, which was large enough to account for variations in the beam profile due to deterioration of the tritiated titanium target. The mean neutron energy calculated from the reaction kinematics with the aid of the neutron beam profile for the target conditions of the

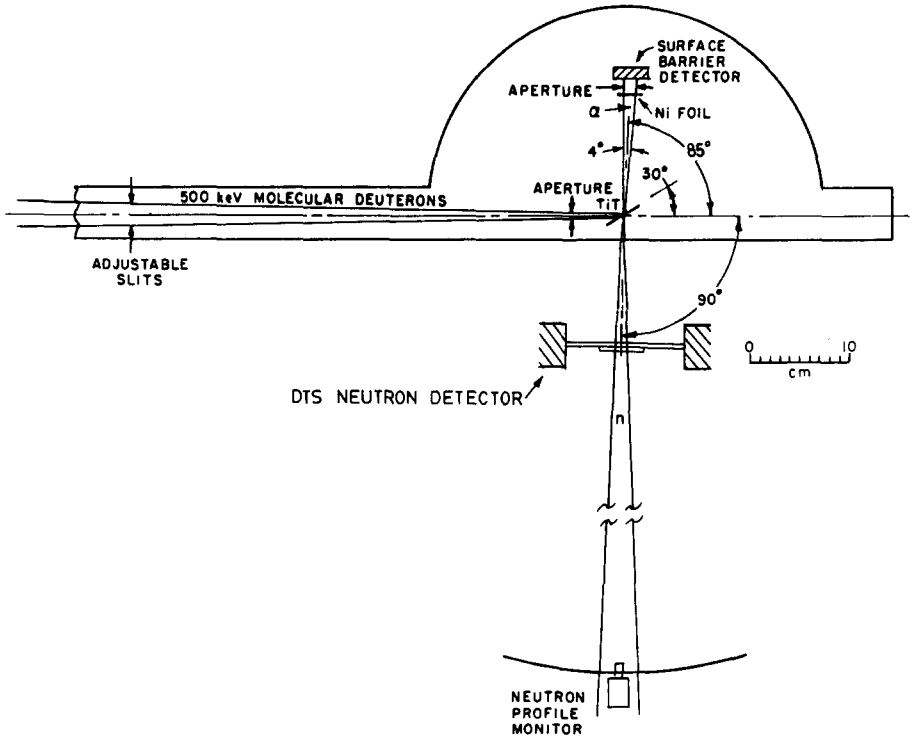

Fig. 6. Experimental geometry used for the neutron detector efficiency calibration at 2.45 and 14.0 MeV.

present experiment was 14.04 ± 0.10 MeV. The correction for the number of neutrons scattered out of the cone was 2.35%.

4.3. Calibration at 2.45 MeV

The experimental geometry at 2.45 MeV which is shown in fig. 6 was essentially the same as the one used for the 14 MeV calibration. In this case the 500 keV D_2^+ molecular ion beam, also collimated to a 3 mm diameter, was incident onto a 0.62 mg/cm^2 thick TiD target positioned at 20° with respect to the deuteron beam axis. The beam current was ~ 0.5 μA on the target. The D(d, n)^{3}H reaction produced a 0.92 MeV ^{3}He associated particle which was detected by a 404 μm thick surface barrier detector located at a 70° angle with respect to the beam axis, and at a distance of 14.6 cm from the target. The ^{3}He detector was collimated to a 1.3° cone half-angle, to produce a ^{3}He counting rate of ~ 40 s^{-1}. A 0.23 mg/cm^2 thick aluminized Mylar foil was placed over the collimator in order to reduce the background and pile up pulses from the elastic scattered deuterons. The background under the selected window for ^{3}He events was measured by inserting a 1.1 mg/cm^2 Ni foil over the detector surface. This foil thickness was sufficient to remove the ^{3}He from the spectrum but caused only a slight shift in the triton peak from the competing D(d, p)T reaction. In order to reduce the neutron scattering corrections no cooling was used in the target. Because of this a shift was observed in the ^{3}He spectrum during the bombardment. The ^{3}He window was changed for different irradiations in order to compensate for the decrease in the ^{3}He yield as a result of target deterioration. The separation of the ^{3}He from the tritons and protons produced in the D(d, p)T reaction was accomplished by pulse height discrimination.

The neutrons were detected at 94° and 99% of the associated neutron flux was contained in a cone subtending a 10° half-angle. The profile was measured by a monitor consisting of a 2.5 cm diameter, 7.5 cm thick NE110 plastic scintillator. Corrections to the measured profile were applied due to target deterioration, and to the finite sizes of the monitor and target beam spot. The cone subtended by the neutron flux detector had a 13.0° half-angle which was sufficiently large to account for variations in the beam profile. The mean neutron energy was calculated from the reaction kinematics for each individual run with the aid of the measured neutron beam profile, and ranged from 2.38 to 2.46 MeV, depending on the target conditions. The average neutron energy for all runs considered was 2.446 ± 0.006 MeV. The number of neutrons scattered in and out of the cone was calculated using cross sections from the ENDF/B-V library [10]. This correction was 4.2%.

4.4. Results of the experimental calibration

Using the time-correlated associated particle technique, the neutron detection efficiency is given by the simple relation:

$$\varepsilon = (Y_c/Y_a) f, \tag{7}$$

where

ε is the detector efficiency,

Y_c is the number of coincidences between the associated particle and the proton recoils,

Y_a is the number of associated particles detected,

f is the total correction factor including: neutron beam attenuation through the materials between the target and the neutron detector, dead time losses, divergence of the neutron beam, associated particle background, and loss of coincidences.

The results of the experimental detector efficiency were carefully compared to a Monte Carlo calculation in order to assess the accuracy of the detector as an absolute flux monitor. This comparison is discussed in section 5. The experimental results are presented for each energy separately.

4.4.1. Results at 14.0 MeV

Fig. 7 shows the ^{4}He associated-particle spectrum obtained with the silicon surface barrier detector. The main peak is the associated-particle events. The solid curve indicates the background obtained with the aluminum absorber. The background for the present experiment was 1.3% of the ^{4}He counts.

Fig. 8 shows proton recoil spectra obtained for 14.0 MeV neutrons. Spectrum A is the proton recoil spectrum corresponding to single events in scintillator 1. This spectrum was obtained by disconnecting the scintillator 2 signal at the input of the sum amplifier. Spectrum B is the coincidence spectrum corresponding to protons that lose a fraction of their energy in each scintillator. This spectrum was obtained using an extra timing leg for scintillator 2, similar to the one used for scintillator 1, and a coincidence unit to trigger the GATE & DELAY activating the time analyzer. Spectrum C is the summed spectrum, which includes protons totally absorbed in scintillator 1 and protons that lose a fraction of their energy inside each scintillator. This spectrum was obtained with the electronics of fig. 5. Spectrum C approximates the thin scintillator response and is the one used to calculate the efficiency. The average number of photoelectrons which would produce the resolution at the spectrum edge (14.0 MeV protons) is 640 ± 32. The solid curves are the theoretical spectra obtained from a Monte Carlo calculation which is discussed in section 5. At 14.0 MeV the fraction of counts due to coincidence events is approximately 54% of the counts in spectrum C above the spectrum bias indicated in fig. 8. This bias corresponds to a proton energy of

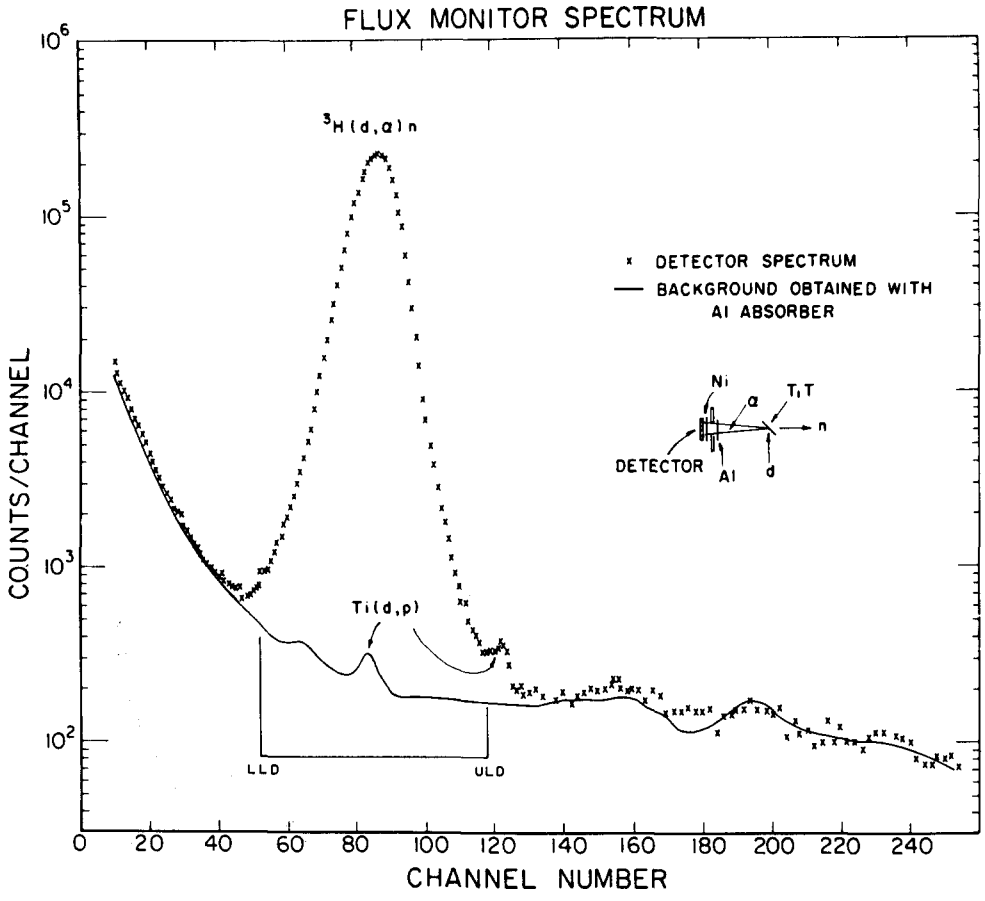

Fig. 7. Spectrum observed in the associated-particle detector for 14.0 MeV neutrons. The labels LLD and ULD denote the discrimination window used for the detector calibration.

4.212 MeV (30% of 14.04 MeV).

There is a small fraction of coincidences which are lost because the signal from scintillator 1 is below the electronic CFD lower level threshold. Some of these lost coincidences have a signal from scintillator 2 which is above the selected spectrum bias used to determine the detector efficiency. Therefore, a correction must be applied for these lost events. This correction was determined by measuring the detector efficiency for several CFD lower level settings. These values were extrapolated to zero CFD lower level threshold by means of the Monte Carlo calculation (see section 5.3).

The results for the experimental efficiency using the spectrum bias at the energy corresponding to 30% of the maximum proton energy (4.212 MeV) are shown in fig. 9. Here the abscissa is the ratio between the pulse height of the CFD lower level and the maximum pulse height, defined as the half height of the spectrum edge. The spectrum drop-off in the CFD lower level region is not a step function, therefore a convolution between a Gaussian function and a straight line was used in order to determine the CFD lower level pulse height more accurately. The solid curve in fig. 9 is the Monte Carlo calculation. The values of typical factors involved in the determination of the experimental efficiency at 14.04 MeV are listed in table 1, together with the associated error in the efficiency. The correction for loss of coincidences is only applied to get the extrapolated efficiency to zero CFD lower level. This correction does not need to be applied if the CFD settings remain the same, and the detector is used at the same neutron energy at which it was calibrated.

The average efficiency for all measurements extrapolated to zero fractional discriminator level (see fig. 9) is 6.97×10^{-3} with an uncertainty of 0.7%.

4.4.2. Results at 2.45 MeV

Fig. 10 shows the ^{3}He associated-particle spectrum together with the spectra of tritons and elastic scattered deuterons obtained by the silicon surface barrier detector. In this figure, the dashed line represents the background spectrum obtained by using the 1.1 mg/cm^2 Ni

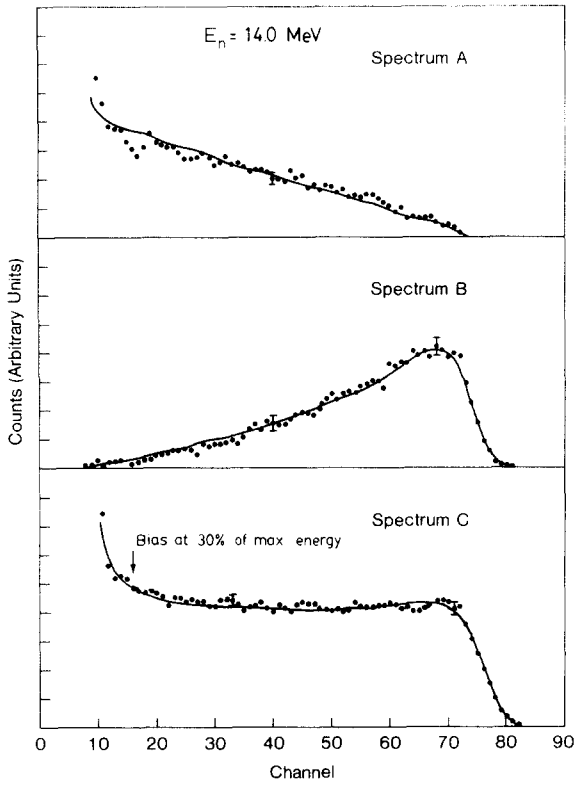

Fig. 8. Experimental proton recoil spectra obtained in an associated-particle experiment at 14.0 MeV. Spectrum A is from the first scintillator. Spectrum B is the sum coincidence of both scintillators. Spectrum C which is the sum of spectra A and B approximates the ideal thin scintillator response. The solid lines are Monte Carlo calculations.

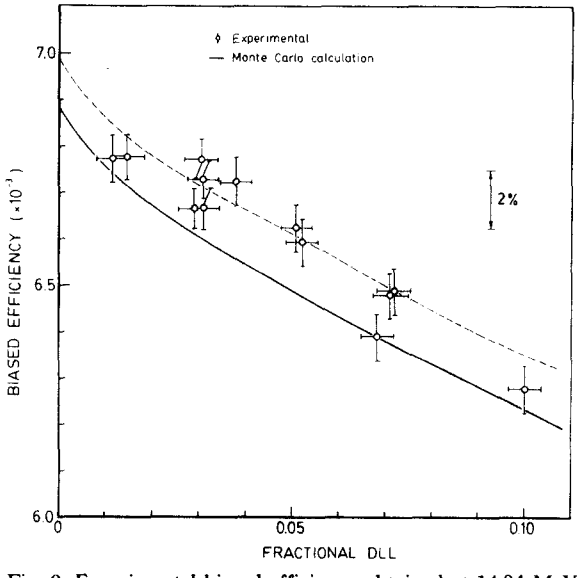

Fig. 9. Experimental biased efficiency obtained at 14.04 MeV. The spectrum bias corresponds to 4.212 MeV proton energy. The solid line is the Monte Carlo calculation. The dashed line represents one standard deviation uncertainty in the calculated curve. The abscissa is the fractional electronic discriminator lower level setting.

Table 1
Typical factors involved in the experimental efficiency at 14.04 MeV at a fractional lower level discriminator of 0.01

Factor	Value	Uncertainty (%)
Y_c / Y_a	6.415×10^{-3}	0.5
Neutron beam attenuation	0.9765	0.3
Dead time correction	1.019	0.1
Devergence of the neutron beam	1.0009	< 0.01
Associated particle background	1.011	0.2
Loss of coincidences	0.984	0.2
Efficiency [a]	6.775×10^{-3}	0.7

[a] Efficiency and uncertainty do not include loss of coincidence correction and its associated uncertainty.

absorber. The window used for the neutron detector calibration is indicated in the figure. The ^{3}He background ranged from 3.4% to 9.4% depending on the target conditions. The ^{3}He counts under the selected window was typically 60% of the triton counts.

Fig. 11 shows the proton recoil spectrum obtained with 2.45 MeV neutrons. The solid line is a Monte Carlo calculation. The average number of photoelectrons corresponding to the spectrum edge (2.45 MeV protons) was deduced to be 75 ± 18. No attempt was made to separately measure the coincidence spectrum between the two scintillators in the neutron detector because of the low target yield. In this case only about 0.5% of the protons escape because of the small range in the scintillator (0.099 mm).

The loss of coincidence events between the two scintillators due to signals which were below the discriminator setting were taken into account. Lost coincidences due to proton escape from scintillator 1 is ~ 0.1%. The majority of coincidences at this energy are due to neutrons which produce recoil events in each scintillator (i.e., double neutron scattering). The fraction of these coincidences which are lost because the signal from scintillator 1 is below the CFD lower level amounts to 4.5% of the total counts. In fact this correction partially compensates for the correction due to multiple scattering.

The results for the experimental efficiency using the spectrum bias at the energy corresponding to 30% of the maximum energy are shown in fig. 12 as a function of the fractional CFD lower level.

The values of typical factors used in the determination of the experimental efficiency at 2.446 MeV are listed in table 2. Using an average of the three measure-

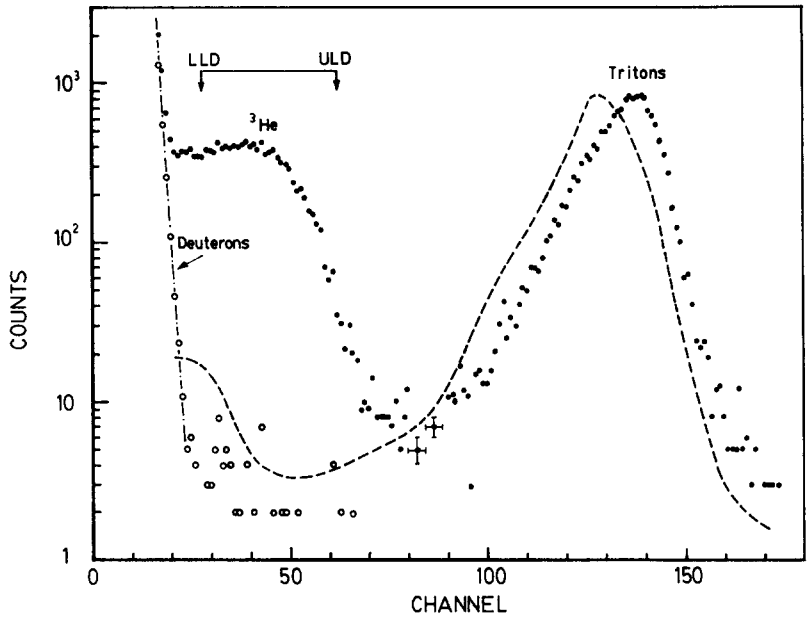

Fig. 10. The experimental spectra obtained in the associated-particle detector at 2.45 MeV. The dashed line indicates the background measured with a thin foil which absorbs the ^{3}He particle but transmits H, D, and T.

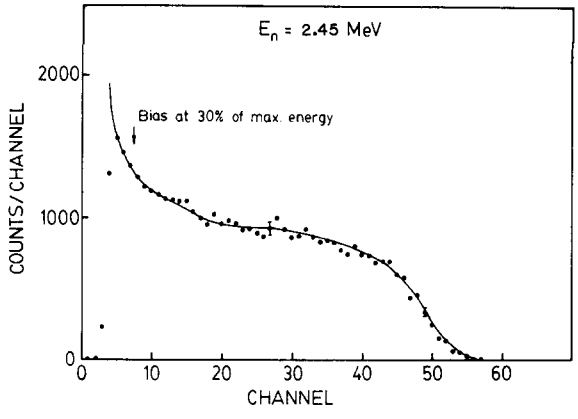

Fig. 11. Proton recoil spectra obtained with 2.45 MeV neutrons in an associated-particle experiment. The solid line is the Monte Carlo calculation.

Table 2
Factors involved in the experimental efficiency at 2.446 MeV at a fractional lower level of 0.078

Factor	Value	Uncertainty (%)
Y_c/Y_a	2.342×10^{-2}	1.0
Neutron beam attenuation	0.958	0.4
Deadtime correction	1.000	< 0.01
Divergence of the neutron beam	1.0058	0.06
Associated particle background	1.052	1.0
Loss of coincidences	0.962	0.5
Efficiency [a]	2.585×10^{-2}	1.6

[a] Efficiency and uncertainty do not include loss of coincidence correction and its associated uncertainty.

ments and extrapolating to zero fractional discriminator level (see fig. 12), the efficiency is 2.69×10^{-2} with an uncertainty 1.5%.

5. Calculated efficiency between 1 and 15 MeV

In order to extend the detector efficiency to cover a broad energy range, a Monte Carlo code has been

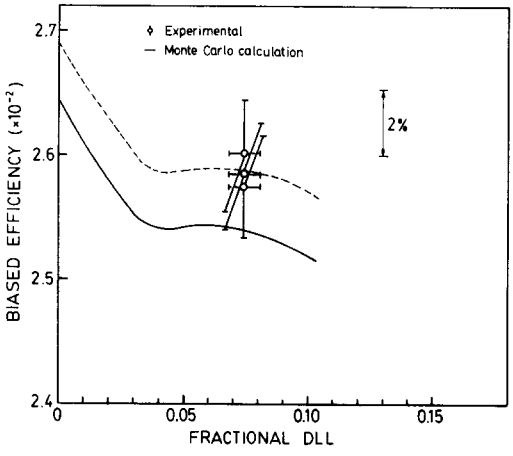

Fig. 12. Experimental biased efficiency obtained at 2.45 MeV. The spectrum bias corresponds to 0.734 MeV. The solid line is the Monte Carlo calculation. The dashed line represents one standard deviation uncertainty in the calculated curve. The abscissa is the fractional electronic discriminator lower level.

developed to calculate the neutron detector efficiency and the expected pulse height distribution of proton recoils as a function of the neutron energy. The computer code CARLO BLACK [11], originally written for use with the "Black Detector", has been modified to be compatible with the characteristics of the present detector. The details of the modifications performed are described in the following sections. The evaluation of the neutron detector efficiency and pulse height distribution at the measured energies 14.0 and 2.45 MeV are given. A method for extending the detector efficiency for other energies in the 1–15 MeV range is presented, together with the estimated uncertainties.

5.1. Improvements in the cross sections

The cross sections for all reactions involved in the energy range of interest (0–15 MeV), were taken from the ENDF/B-V library [12,13]. The reactions are: H(n, n)H, C(n, n)C, ^{12}C(n, n'γ)^{12}C, ^{12}C(n, α)^{9}Be, and ^{12}C(n, n')3α.

The angular distribution for the C(n, n)C reaction was also taken from the ENDF/B-V evaluation. Since the coefficients for the Legendre polynomial expansion are given in the center-of-mass system, a transformation to the laboratory system was performed to be compatible with the Monte Carlo code. The following relationship was used for this purpose [14]:

$$w_l' = \sum U_{lm}^{*} w_l, \tag{8}$$

where U_{lm}^{*} is the transformation matrix taken from the ENDF/B-V evaluation and w_l', w_l are the Legendre polynomial coefficients in the laboratory and center-of-mass systems, respectively.

The angular distribution for the H(n, n)H reaction was taken from Hopkins and Breit [15]. The interpolation procedure between the energies found in the table was similar to the one used for the C(n, n)C angular distribution.

5.2. The scintillator light response for protons

The NE110 scintillator relative light response was measured for proton recoils in the energy range between 0.52 and 14 MeV using the NBS 150 MeV Electron Linac as the source of neutrons. The time-of-flight technique was used on the 200 m flight path. Two parameter data, consisting of 1024 pulse-height channels and 512 time-of-flight channels (64 ns/channel time width) were accumulated for the neutron detector. The gamma flash from the LINAC tungsten target was the timing reference for the definition of the neutron energy scale. A check on the neutron energy calibration was performed, previous to this experiment, using the well defined 2078 keV carbon resonance. The results of this check showed good agreement ($\sim 0.3\%$) with the calculated neutron energy.

The channel a maximum proton recoil energy was determined by a least-squares fitting for each of forty-three spectra with Monte Carlo calculations. Corrections for relativistic effects and neutron yield variation with time-of-flight were applied to obtain the neutron energy. The nonlinearity of the electronic system was measured and used to correct the values of the edge channels, determined from experimental spectra. A least square fit between the measured response and the proton energy was performed using the following function:

$$\ln(P) = \sum_{i=0}^{5} a_i [\ln E]^i, \tag{9}$$

where

P is the measured relative light response,

E is the proton energy (MeV), and

a_i are the fitted coefficients.

The results for the relative light response are shown in fig. 13 as a function of the neutron energy. The measured response was normalized to the values from the code 05S [16] in the region between 2.0 and 2.8 MeV for the sake of comparison. There is an overall agreement with the values from 05S within the estimated error of the present measurements ($\sim 2\%$). The agreement below 4.0 MeV is better than 1.5% except for the

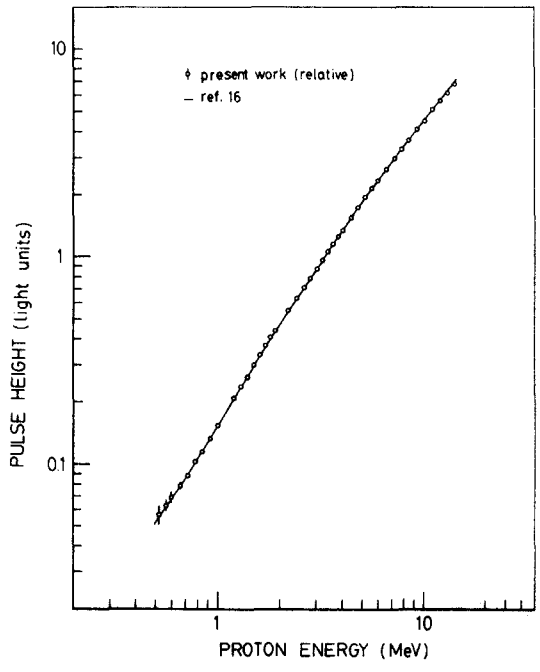

Fig. 13. Relative light response of the NE110 scintillator with proton energy. The solid line is from code 05S [16]. The experimental points were normalized in the 2.0–2.8 MeV region.

three lowest points which have larger errors due to an uncertainty in the ADC channel zero determination. These results agree with those from Renner et al. [17] which were also obtained using a NE110 plastic scintillator.

5.3. The effect of lost coincidences

The escape of protons from the forward face of the first scintillator is a large effect at energies greater than several MeV. However, the corresponding distortion in the proton recoil spectrum is eliminated experimentally with the detection of the escaped protons by the second scintillator which is located behind the first one. Because this process requires a coincidence signal, there is a lower limit for the detectable pulse height in the first scintillator. The pulses below this limit will be lost. Some of these lost coincidences could produce sum pulses above the selected bias, therefore a correction for this effect is necessary. At low neutron energies there is also loss of coincidences due to multiple scattering between the two scintillators which has to be taken into account.

The effect of lost coincidences for the escape of protons was incorporated in the Monte Carlo code by calculating the fraction of the proton energy which is deposited in each of the scintillators. In this calculation the range–energy relationships were taken from Cecil et al. [3] for protons above 0.5 MeV, and from Watson and Graves [18] for protons below 0.5 MeV.

The total light produced by a given neutron in the Monte Carlo code was separated into two parts: the first corresponding to the total light produced inside the first scintillator and the second corresponding to the total light produced inside the second scintillator. The events that produced light in the first scintillator below a selected threshold value were rejected. In this manner the loss of coincidences due to multiple scattering was also considered.

The correction for lost coincidences is plotted in fig. 14 as a function of the fractional discriminator lower level, for several incident neutron energies. Here the discrimination channel for the efficiency calculation was set at 30% of the maximum proton energy.

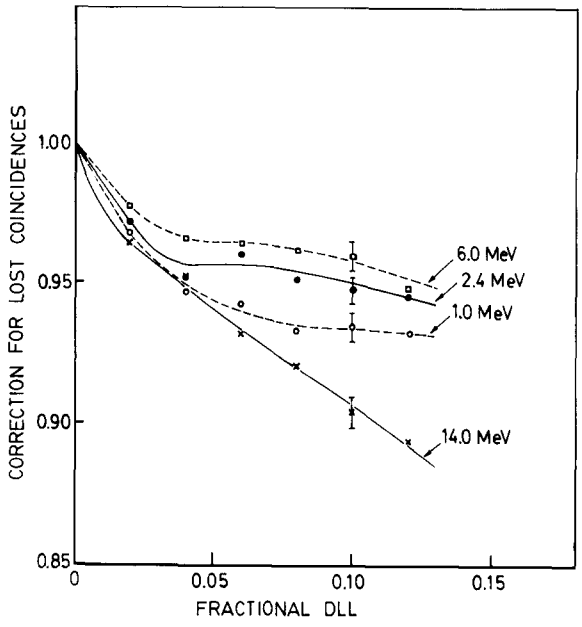

Fig. 14. Correction for lost coincidences at several incident neutron energies. The efficiency was calculated with a bias at 30% of the maximum energy.

5.4. Variation in light collection

As pointed out in section 3.3, the variation in the light collection has been measured at different points of each scintillator. This effect, although small, was incorporated in the Monte Carlo code by using the following expression:

$$P(r) = P(0)(1 + ar^2), \tag{10}$$

where $P(r)$ is the light response at a distance r(cm) from the center of the scintillator and a is the coefficient deduced from the measured variation in light collection at $r = 1$ cm for each individual scintillator. The measured average values for a were 0.0107 for scintillator 1 and 0.0040 for scintillator 2.

5.5. Pulse height resolution

The pulse height distribution calculated by the Monte Carlo code was fitted to the experimental proton recoil spectra by means of a code written by Meier [19] which takes into account the Poisson statistics in the number of photoelectrons detected. The photoelectron conversion efficiency (keV/photoelectron which determines the Poisson spreading) and a channel width ratio (determining the relative horizontal gain) are the two input parameters which can be varied freely or under the constraint that calculation and experiment have the same spectral area within a given pulse height range.

5.6. Forced first collision technique

The present detector has a high transmission for MeV neutrons. This results in a low detection efficiency. Therefore, a large number of incident neutrons would be required in the Monte Carlo calculation in order to have sufficient statistical accuracy and a long processing time would then be necessary. This problem was solved by using the forced first collision technique [20]. In this case the position for the collision ($0 \leqslant l \leqslant L$) is given by:

$$l = -\lambda \ln\{1 - r[1 - \exp(-L/\lambda)]\}, \tag{11}$$

where

λ is the average distance to the first collision,

r is a random number in the interval $0 \leqslant r \leqslant 1$,

L is the total length of the detector (scintillator 1 + scintillator 2).

This results in 100% detection efficiency which considerably decreases the processing time. A proper transmission factor is then applied to this calculated efficiency.

5.7. Interactions in the materials around the scintillators

In order to determine the absolute efficiency with good accuracy it is desirable to keep small the correction factors involved. The presence of materials around the scintillators introduces some small effects in the efficiency that have to be considered. The aluminum wrapping the scintillators and in the detector window produces a negligible attenuation of the neutron beam ($< 0.1\%$) for the energy range considered here. Alpha particles from the $^{27}Al(n, \alpha)^{24}Na$ reaction produce low light output and are eliminated by pulse height discrimination. Protons from the $^{27}Al(n, p)^{27}Mg$ reaction increase the efficiency by only $\sim 0.05\%$ at 15 MeV and less for lower energies.

The aluminum between the two scintillators absorbs a small fraction of the proton's energy, distorting the proton recoil spectrum in the second scintillator. This effect has been calculated to $\sim 0.05\%$ and was therefore neglected.

Additional variation in the efficiency is possible due to neutron interactions in the plexiglas light guide and phototube glass. The magnitude of this effect depends on the size of the neutron beam compared to the scintillator. Neutrons scattered once by the scintillator can go to the plexiglas or phototube and be scattered back into the scintillator. For a case where the neutron beam is smaller than the scintillator, this effect is small because of the detector dimensions. Contribution from the plexiglas was estimated to be $\lesssim 0.04\%$ and from the phototubes $\lesssim 0.02\%$.

In the case where the neutron beam is larger than the scintillator, this effect is larger, but can be reduced if a collimator slightly larger than the scintillator is used. For a collimator diameter 1 cm larger than the scintillator diameter the contribution from C(n, n)C scattering has been estimated to be $\sim 0.5\%/b$. The reaction H(n, n)H contributes both protons and neutrons to the scintillator. If the efficiency is calculated for a bias corresponding to 30% or more of the maximum energy, only a fraction of these events will contribute to the efficiency. The contribution from neutrons is maximum for the lowest energy, being around 0.2% at 1 MeV. The contribution from protons increases with the energy due to the larger range in the scintillator. Because the light guide has a hydrogen concentration comparable to NE110, the incoming protons from the edge of the scintillator are compensated almost exactly by the outgoing protons from the scintillator. The net effect is expected to be $\sim 0.5\%$ at 15 MeV, and smaller at lower energies.

5.8. Results of the calculations

The behavior of the calculated biased efficiency with neutron energy follows essentially the H(n, n)H cross section. Contributions from C(n, n)C and $^{12}C(n, n'\gamma)^{12}C$ cross sections cause some small irregularities in the efficiency curve, mainly in the regions of carbon resonances. The efficiency curve is shown in fig. 15, together with the experimental points at 2.45 MeV and 14.0 MeV. The experimental points are the averages at each energy extrapolated to zero fractional discriminator level. For this curve the bias energy was located at 30% of the maximum energy.

A clear correlation between the biased efficiency and the carbon and hydrogen cross sections was observed. Particularly, good accuracy in interpolation of the efficiency for various neutron energies was obtained using the following formula:

$$\varepsilon_B/\sigma_H = a_1 + a_2\sigma_c + a_3\sigma_H, \tag{12}$$

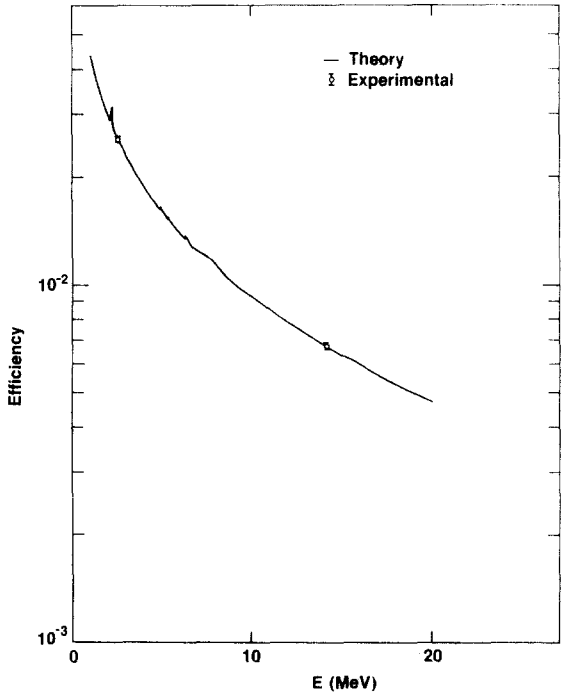

Fig. 15. Detector biased (30% of the maximum proton energy) efficiency curve. The points at 2.45 MeV and 14.0 MeV were obtained experimentally. The solid line is the Monte Carlo calculation.

where

ε_B is the biased efficiency,

σ_C is the carbon elastic plus inelastic scattering cross sections,

σ_H is the H(n, n)H cross section,

a_1, a_2, a_3 are constants.

The values of a_1, a_2 and a_3 were obtained by least-squares fitting between ε_B/σ_H and the cross sections. The biased efficiency has been calculated at several selected energies, where the carbon cross section shows largest variations. The results of the fittings are presented in table 3 using the following fractional bias energies: 0.30, 0.35, and 0.40 of the maximum energy. These efficiencies were calculated at zero discriminator lower level. The average accuracy obtained in the interpolation goes from 0.8% to 1.8% at the fractional biases 0.30 and 0.40, respectively.

The value of a_1 corresponds to the biased efficiency without multiple scattering correction, in b^{-1}. The values of a_2 and a_3 correspond to the multiple scattering correction in carbon and hydrogen, respectively, in b^{-2}. The value of a_2 decreases with the fractional bias energy, whereas a_3 increases. This behavior is explained by the variation in the spectrum shapes due to multiple scattering. For carbon, the counts are shifted to lower pulse amplitudes, whereas for hydrogen, the counts are shifted to higher pulse amplitudes [1].

Fig. 16 shows the uncertainties involved in the calculated efficiency. The multiple scattering correction is predominant from 1.0 to 4.5 MeV. Above this energy, the uncertainty in the H(n, n)H cross section becomes predominant up to 15 MeV. The uncertainty in the correction for lost coincidences has not been included in fig. 16 since it depends on the discrimination level used. This uncertainty is estimated to be around 10% of the correction (i.e., ~ 0.4%) and has little contribution in the total uncertainty. The total uncertainty is $\lesssim 1.5\%$ above 4.0 MeV. It is between 1.4 and 2.1% for 1.0–4.0 MeV except near the narrow resonance in the C(n, n)C cross section at 2.078 MeV where it reaches the maximum value of 2.6%.

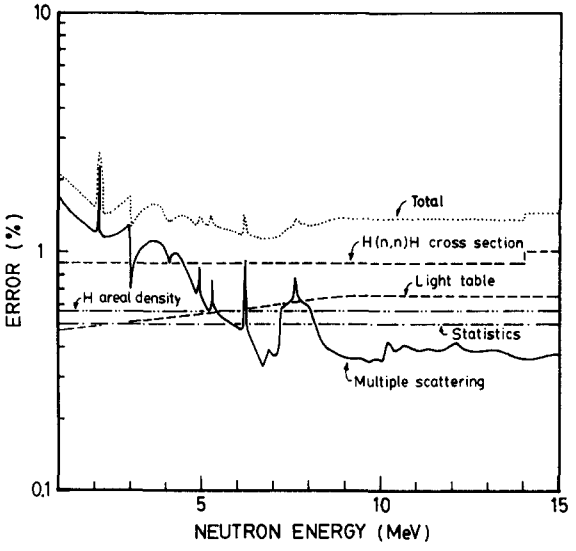

Fig. 16. Summary of statistical and systematic uncertainties for the neutron detector efficiency calculation.

5.9. Comparison between calculated and experimental efficiencies

The following procedure was used to compare the calculated and measured proton recoil spectra at 14.0 and 2.45 MeV. The light distributions from the Monte Carlo code were initially corrected for nonlinearity in the experimental electronics. The calculated spectra were then smeared by a Poisson resolution function and fitted to the experimental spectra with the aid of the code FIT978 [19]. From these fits the values of the experimental and calculated efficiencies were obtained. Comparisons between theory and experiment are shown in figs. 9 and 12 for 14.0 and 2.45 MeV neutrons for several runs at different discriminator settings. There was excellent agreement between the calculated and experimental efficiencies for a wide range of bias energies.

From the results it can be observed that on the average, the theoretical and experimental efficiencies agree with each other within the estimated uncertainty in the theory which is ~ 1.7% (one standard deviation).

Table 3
Interpolation parameters for the calculated efficiency

Fractional bias energy	Interpolation parameter			
	a_1 ($\times 10^{-3}$ b^{-1})	a_2 ($\times 10^{-4}$ b^{-2})	a_3 ($\times 10^{-4}$ b^{-2})	Reduced χ^2
0.30	9.364	3.293	1.356	1.0
0.35	8.667	2.928	1.610	0.77
0.40	7.817	2.788	2.128	2.8

In comparing the theoretical and experimental spectra at 14.0 MeV neutron energy a difference in the alpha peak position and shape was observed. This peak which is located at the low pulse amplitude region of the proton recoil spectrum originates from the $^{12}C(n, \alpha_0)^9Be$ reaction in the scintillator. The dominant cause of this difference was attributed to a variation in the light output for alpha particles from that originally used in the calculation [16]. This difference has been corrected by increasing the light output for alpha particles by 30%. A less important contribution to the shape of the alpha peak was the anisotropy in the $^{12}C(n, \alpha_0)^9Be$ angular distribution. This effect has not been accounted for in the present calculation. However, it has no effect in the detection efficiency since the spectrum bias can always be chosen above the alpha peak channel.

Since the 0.7% uncertainty in the measured efficiency at 14.0 MeV is less than the 1.7% uncertainty in the calculation, the calculation is normalized to the experiment at this energy. This increases the calculated efficiency by 1.3% at all neutron energies. The resultant uncertainty in the detector efficiency is thus 0.7% at 14.0 MeV and increases to 1.5% at the lower neutron energy of 2.45 MeV.

6. Summary

A dual thin scintillator has been designed and calibrated to be used as an absolute flux monitor for 1–15 MeV neutrons. The detector eliminates experimentally the distortion due to the escape of protons and also has a low multiple scattering correction. The detector may be used in transmission geometry and without precision collimators when necessary. The experimental absolute detector efficiency was measured at 14.0 and 2.45 MeV. A Monte Carlo code was developed for calculating the absolute detector efficiency for the 1–15 MeV energy range. The agreement between the theoretical and experimental efficiencies was within the error in the theory which was around 1.7%. A good agreement was observed between the theoretical and experimental proton recoil spectrum shapes. The uncertainty in the calculated efficiency was estimated to be between 1.4 and 2.1% for the 1–15 MeV energy region, except in the region of the narrow resonance in the C(n, n)C reaction at 2.078 MeV, when the uncertainty reaches a maximum of 2.6%.

We would like to thank R.S. Caswell and C.D. Bowman for their support and interest, K.C. Duvall for his assistance at the NBS Van de Graaff accelerator, J. Whittaker for his electronic assistance, and R.A. Schrack, A.D. Carlson, J.W. Behrens and J. Coyne for their valuable comments. We are especially indebted to J.B. Czirr for introducing the thin-scintillator concept to us and for his continued interest throughout its development.

References

[1] D.W. Jones and M.E. Toms, Naval Research Laboratory Report 7324 (1971).
[2] Nuclear Enterprises Inc., Brochure 126P (February 1980).
[3] R.A. Cecil, B.D. Anderson and R. Madey, Nucl. Instr. and Meth. 161 (1979) 439.
[4] J.F. Janni, Air Force Weapons Laboratory Report AFWL-TR-65-150 (September 1966).
[5] C.H. Johnson, Fast neutron physics, part 1, ch II.C, eds., J.B. Marion and J.L. Fowler (Interscience, New York, 1960) p. 247.
[6] D.G. Crabb, A.J. Dean, J.G. McEwen and R.J. Ott, Nucl. Instr. and Meth. 45 (1966) 301.
[7] M. Salomon, Nucl. Instr. and Meth. 153 (1978) 289.
[8] K.C. Duvall and O.A. Wasson, IEEE Trans. Nucl. Sci. NS-28 (1981) 1488.
[9] O.A. Wasson, A.D. Carlson and K.C. Duvall, Nucl. Sci. Eng. 80 (1982) 282.
[10] ENDF/B-V, Report BNL-NCS-1754 (ENDF-201), ed., R. Kinsey, available from the National Nuclear Data Center, Brookhaven National Laboratory, Upton, NY (July 1979).
[11] W.P. Poenitz, The black neutron detector, Argonne National Laboratory Report ANL-7915 (April 1972).
[12] ENDF/B-V data file for ^1H(MAT 1301), evaluation by L. Stewart, R.J. LaBauve and P.G. Young (LANL), BNL-NCS-17541 (ENDF-201), ed., R. Kinsey, available from the National Nuclear Data Center, Brookhaven National Laboratory, Upton, NY (July 1979).
[13] ENDF/B-V data file for ^{12}C(MAT 1306), evaluation by C.Y. Fu and F.G. Perey (ORNL), BLN-NCS-17541 (ENDF-20), ed., R. Kinsey, available from the National Nuclear Data Center, Brookhaven National Laboratory, Upton, NY (July 1979).
[14] ENDF/B-V, Report BNL-NCS-50496 (ENDF-102), ed., R. Kinsey, available from the National Nuclear Data Center, Brookhaven National Laboratory, Upton, NY (October 1979).
[15] J.C. Hopkins and G. Breit, Nucl. Data Tables A9 (1971) 137.
[16] R.E. Textor and V.V. Verbinski, RSIC computer code collection, PSR-14 (1968, documentation updated September 1973).
[17] C.Renner, N.W. Hill, G.L. Morgan, K. Rush and J.A. Harvey, Nucl. Instr. and Meth. 154 (1978) 525.
[18] J.W. Watson and R.G. Graves, Nucl. Instr. and Meth. 117 (1974) 541.
[19] M.M. Meier, National Bureau of Standards Internal Report (February 1978).
[20] E.D. Cashwell and C.J. Everett, A practical manual on the Monte Carlo method and random walk problems (Pergamon, New York, 1960) p. 30.